Methods xxx (xxxx) xxx

Contents lists available at ScienceDirect

Methods

journal homepage: www.elsevier.com/locate/ymeth

Atomic force microscopy for quantitative understanding of peptide-induced lipid bilayer remodeling

K.G. Schaefer [a], A.E. Pittman [a,1], F.N. Barrera [b], G.M. King [a,c,*]

[a] Department of Physics and Astronomy, University of Missouri-Columbia, Columbia, MO 65211, USA
[b] Department of Biochemistry & Cellular and Molecular Biology, University of Tennessee, Knoxville, TN 37996, USA
[c] Department of Biochemistry, University of Missouri-Columbia, Columbia, MO 65211, USA

ARTICLE INFO

Keywords:
Pore forming
AFM
Scanning probe
Supported lipid bilayer
SLB

ABSTRACT

A number of peptides are known to bind lipid bilayer membranes and cause these natural barriers to leak in an uncontrolled manner. Though membrane permeabilizing peptides play critical roles in cellular activity and may have promising future applications in the therapeutic arena, significant questions remain about their mechanisms of action. The atomic force microscope (AFM) is a single molecule imaging tool capable of addressing lipid bilayers in near-native fluid conditions. The apparatus complements traditional assays by providing local topographic maps of bilayer remodeling induced by membrane permeabilizing peptides. The information garnered from the AFM includes direct visualization and statistical analyses of distinct bilayer remodeling modes such as highly localized pore-like voids in the bilayer and dispersed thinned membrane regions. Colocalization of distinct remodeling modes can be studied. Here we examine recent work in the field and outline methods used to achieve precise AFM image data. Experimental challenges and common pitfalls are discussed as well as techniques for unbiased analysis including the Hessian blob detection algorithm, bootstrapping, and the Bayesian information criterion. When coupled with robust statistical analyses, high precision AFM data is poised to advance understanding of an important family of peptides that cause poration of membrane bilayers.

1. Introduction

1.1. Pore-forming peptides

Lipid membranes line the surface of cells and intracellular organelles, providing a semi-permeable barrier that prevents uncontrolled flow of molecules. Soluble peptides can bind to the surface of membranes breaking the barrier to diffusion, often through a complex set of steps leading to the formation of transmembrane pores. Evolution has taken advantage of this process to disrupt membrane integrity in a way that is useful to the organism. A few examples include human antimicrobial peptides that constitute an essential element of the innate immune response [1], melittin, the primary active component of bee venom which causes cellular damage [2], or Candidalysin, which is necessary for the fungal pathogen *Candida albicans* to infect cells in human mucosal tissues [3].

Not only are membrane permeabilizing peptides intriguing from the perspective of understanding the mechanistic basis of their function, but they also hold significant potential for applications across biotechnology and medicine [1,4]. Such applications include delivering of molecular cargo to cells and novel cancer treatments. A fundamental peptide-induced membrane defect is a pore, or a highly localized void in an otherwise continuous lipid bilayer. Diffuse membrane thinning and linear trench-like features as well as other defect modes have been observed [5–7]. Some examples of remodeling modes including pore-like voids, trenches, and membrane-thinned regions are shown in Fig. 1.

The bilayer remodeling process is intrinsically "noisy". Stochastically driven peptides and lipid molecules interact with each other and between themselves on a complex energy landscape that produces stable membrane structures [1,8,9]. Local electric fields, hydrophobic effects, and peptide structure are thought to play important roles in the remodeling process. A number of bulk biochemical techniques can be employed for studying pore formation. Measurements of chemical leakage across unilamellar vesicles are especially powerful, as are electrical recordings [1]. Though bulk methods are in widespread use, they generally leave unresolved the difficult-to-synchronize molecular

* Corresponding author at: Department of Physics and Astronomy, University of Missouri-Columbia, Columbia, MO 65211, USA.
E-mail address: kinggm@missouri.edu (G.M. King).
[1] Current address: St. Jude Children's Research Hospital, 262 Danny Thomas Pl, Memphis, TN 38105, USA.

https://doi.org/10.1016/j.ymeth.2020.10.014
Received 16 September 2020; Received in revised form 17 October 2020; Accepted 20 October 2020
Available online 24 October 2020

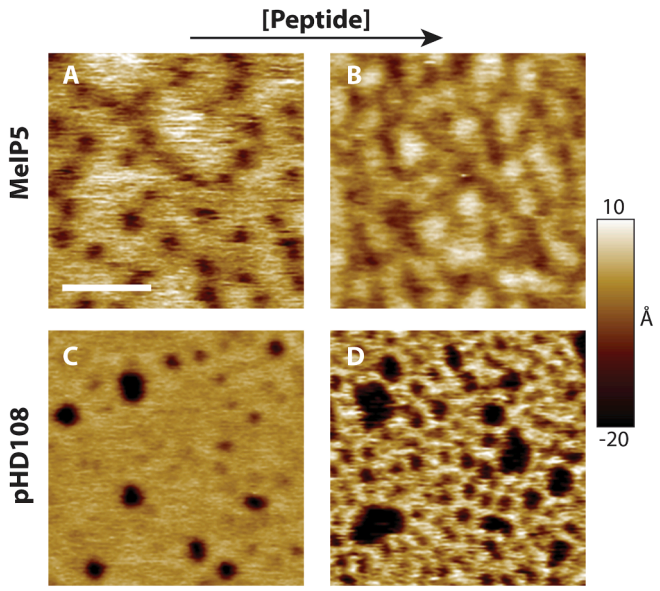

Fig. 1. Pore-forming peptides at work. AFM imaging of supported lipid bilayers subject to MelP5 or pHD108 reveals diverse lipid bilayer remodeling. (A) POPC upon incubation with MelP5 (approximate P:L = 1:1000). Dispersed areas of thinned membrane (*light brown*) adjoin highly localized pore-like voids in the membrane (*dark brown*). Regions exhibiting heights commensurate with the top of the upper bilayer leaflet are also visible (*white*). (B) Image at higher MelP5 concentration (approximate P:L = 1:100). Larger scale linear features (trenches) appear to be favored over highly localized voids. (C,D) Images in acidic buffer (pH 4) reveal remodeling of POPC by the pHD108 peptide at approximate P:L of 1:100 and 1:80, respectively. The lateral scale bar shown in (A) is 50 nm and applies to all panels; the false color vertical scale spans 30 Å, as indicated. Data in (A-C) adapted from refs [27,28].

activities that underlie peptide-lipid interactions. Hence, single molecule investigations are poised to provide valuable insights [1,10,11].

1.2. Single molecule atomic force microscopy of pore forming peptides

A powerful single-molecule technique for direct visualization of biological systems is the atomic force microscope (AFM). Since its original development in 1986 [12], the AFM was adapted to operate in fluid, rendering the instrument capable of physiologically relevant imaging. This opened the door for biophysical studies of membranes in near-native conditions [13]. Though the instrument is capable of atomic resolution when imaging extremely flat surfaces [14], AFM images of complex biological macromolecules are limited by convolution of the tip geometry with that of the specimen. AFM images of membrane proteins have spatial resolution of ~10 Å laterally and ~1 Å vertically [13]. The temporal resolution of the AFM is also important. Imaging frame rates of commercial AFMs can now exceed 10 images per second, though the fundamental "speed limit" of the method can be much faster (~1 μs) [15], as dictated by the mechanical response time of the cantilever which sets an operative lower limit for pixel dwell time. This combination of attributes enables the AFM to directly visualize conformational dynamics, parse asynchronous behavior, and reveal topographical details and heterogeneities that are often blurred out in traditional bulk measurements [16–18].

Supported lipid bilayers (SLBs), robust mimics of biological membrane, are commonly imaged in the AFM [19,20]. Many groups have focused on phase-transitions of different lipid species, as well as remodeling caused by the addition of detergents or peptides [19,21–23]. Poration in membranes has been observed for several peptides, and examples include amyloid β [24,25], the bee venom melittin and derivatives thereof [26–28], and others [7,10,29].

Here we present methods commonly employed in the King laboratory to prepare AFM samples, acquire images, and objectively analyze peptide-induced lipid bilayer remodeling. A recurring challenge when applying this powerful single molecule imaging tool is to measure molecular activities as accurately as possible without sacrificing the biological relevance of the data.

2. Acquiring high precision AFM data in biologically relevant conditions

2.1. Sample preparation considerations

To mimic physiological conditions, peptide-induced membrane remodeling is observed in supported lipid bilayers immersed in aqueous buffer solution. The choice of buffer will influence numerous aspects of the imaging session. Ionic strength mediates the double-layer interaction between the AFM tip and the sample surface. The screening distance between tip and sample depends on salt concentration and valency of the ions in the solution [30,31]. It should also be noted that salt conditions can potentially affect the structure of the peptide under study [32]. The pH of the buffer must also be considered. In many cases, physiological pH is desired (pH 7.0–7.5). However, some intriguing peptides have pH-dependent behavior [7,28,33,34], thus the acidity of the buffer must be tuned accordingly.

Lipid species is another important consideration when imaging peptide-lipid interactions. In the King laboratory we commonly use 1-palmitoyl-2-oleoyl-*glycero*-3-phosphocholine (POPC) or 1,2-dioleoyl-*sn-glycero*-3-phosphocholine (DOPC) as model lipids. Both are zwitterionic and routinely used membrane bilayers in biophysical studies [35-37]. Lipid mixtures that contain a significant fraction of charged headgroups (such as those extracted from *E. coli*), can also be employed [16,17,38], but in some cases these are challenging to form homogeneous SLBs. The effects of phase-coexistent lipids have also been studied [26]. SLBs are typically formed in these experiments through the rupture and absorption of lipid vesicles onto a solid-state surface (see Section 2.1.3) [39].

2.1.1. Liposome preparation

To prepare the liposomes, lipid stock suspended in chloroform (Avanti Polar Lipids) in a glass tube is dried with argon gas to create a film. The tube is then incubated overnight in a vacuum chamber. Following swelling in buffer, the lipids are extruded 25–30 times through ~100 nm diameter filters (Whatman) to create vesicles. Generally, the swelling buffer is the same as the imaging buffer (described in Section 2.1.3). Each batch of lipid stock is quantified using an appropriate assay, such as the Bartlett assay to measure the amount of phosphorus. Careful quantification of lipid concentration is important to deducing the peptide-to-lipid molar ratio (P:L). This ratio is a central factor that influences lipid remodeling and can be a significant source of uncertainty in AFM measurements, as discussed below. Another factor that can affect pore-formation is the size of the liposome itself [40]. Extrusion through varied diameter filters can control for this and the size may be evaluated using dynamic light scattering [41].

2.1.2. Protein-to-lipid ratio considerations

Multiple pore-forming peptides such as melittin have been characterized via leakage and other solution assays at particular P:L values. When addressing the same systems via AFM, previously studied P:L values from bulk measurements represent logical starting points; however, there are a few AFM-specific complications to consider. The initial P:L values can be determined with accuracy if the equilibrium partition coefficient of the peptide into the specific lipid is known. Yet, AFM sample preparation often requires rinsing to minimize loosely bound material that can adhere to or interfere with the tip and cause imaging artifacts [42]. Rinsing removes quantities of peptide, lipid or both. The density of the peptide on the bilayer is challenging to calculate, since it will be a factor of the number and volume of the rinses, as well as the hydrodynamic properties of the flow (laminar vs. turbulent), which are

complicated by surface effects. As a result, even if the dissociation constant is known, errors in the estimated P:L can be large. In principle, rinse volumes can be analyzed to measure the amount and type of material removed during each rinsing step, but this is challenging due to small overall volumes and is not often performed. Additionally, even if the P:L is known, it may need to be modulated from bulk values to optimize single molecule data collection. In practice, we have found it best to evaluate a broad range of initial P:L (for example, from 1:50 to over 1:1000) in order to find conditions where pore-like features are visible, well-separated, and abundant enough for robust quantification [27]. The range of optimal P:L values for AFM imaging may be narrow, making this an important step when approaching a new sample.

It is important to note that while the overall P:L can be controlled at the initial stages of sample preparation, it is difficult to account for or to predict the effects of rinsing as well as overall sample inhomogeneity or incomplete mixing. A common question arises as to whether or not the P:L ratio is uniform on a given surface. Despite thorough mixing and rinsing prior to AFM imaging we have observed significant bilayer remodeling variations occurring across small length scales (~150 nm) on the exact same sample surface (Fig. 2). Local inhomogeneities can persist. Observation of asynchronous bilayer remodeling activity suggests the importance of local concentration gradients in remodeling activity.

2.1.3. Surface incubation methods

Standard protocols for the formation of SLBs are adapted for AFM studies. They require that a given concentration of liposomes (typically, 100 μM DOPC) are deposited on freshly cleaved mica, incubated for a period of time, then rinsed to remove unruptured or loosely bound lipid. Peptide of synthetic or natural origin may be added to the liposomes for incubation prior to deposition onto the solid-state surface, or to a preformed supported bilayer, or a hybrid approach is also possible. In all experiments, mica is the surface of choice because when freshly cleaved, it is clean, atomically flat over large areas, and highly hydrophilic. There are other commonly employed surfaces in biological AFM such as glass, but this often contains pits that are topographically similar to features formed by pore-forming peptides [43].

For a solution-based peptide addition (Fig. 3A), a liposome stock is diluted in imaging buffer that approximates physiological conditions (typically, 10 mM Hepes, 150 mM NaCl, pH 7.5). Peptide is added to the lipid solution and incubated to deliver a specific P:L (typically, 1:100). The liposome-peptide solution is mixed manually with a pipette to ensure uniform diffusion of the peptide. A volume (typically, 75 μL) of the liposome-peptide mixture is then deposited onto freshly cleaved mica. During a surface incubation time of about 10 min at room temperature, bilayers are formed through vesicle fusion [39]. The sample is then rinsed by exchanging 75 μL of imaging buffer with a pipette tip 5 times.

An alternative method consists in adding peptide after the bilayer has formed on the surface (Fig. 3B). In this method, bilayers are formed by absorbing liposomes to freshly cleaved mica for about 15 min. The sample is then rinsed with the imaging buffer and can also be imaged at this stage to characterize the bare lipid. At a later time, peptide is added to the preformed bilayer and incubated. The sample is imaged with or without additional rinsing, as desired.

In some cases, we have also found useful a hybrid incubation method which was inspired by sample preparation protocols developed for nucleic acid imaging [44]. Here peptide is added during the SLB formation process (Fig. 3C). Under certain conditions (i.e., ionic strength, pH, different protein and lipid species, etc.) free peptides can compete successfully with liposomes for binding the supporting surface and thus interfere with bilayer spreading. This method was developed in effort to push such systems in favor of SLB formation rather than coverage of the mica surface with peptide. For hybrid incubation, liposomes are deposited on freshly cleaved mica. A short time (⩽5 min) thereafter peptide is added to the sample. The sample is then incubated ~ 15 min. To ensure uniform diffusion of the peptide, the solution is mixed halfway through this incubation by inserting a pipette tip into the droplet above the surface and depressing and releasing the pipette several times. Then the sample is rinsed in the same manner as the other methods and imaged.

2.2. Imaging

2.2.1. General considerations

When imaging lipid bilayer remodeling, perturbations of the system emanating from the AFM probe tip must be minimized. We typically image using a commercial AFM apparatus (Asylum Research, Cypher) in amplitude modulated intermittent contact (also known as tapping) mode. Careful monitoring of the feedback parameters is critical to minimize the force imparted on the sample (≤100 pN). Since hydrodynamic and thermal perturbations can destabilize measurements performed in fluid, the resonant frequency and amplitude should be checked frequently throughout imaging. It should be noted that though the AFM is capable of imaging individual integral and peripheral membrane proteins, such as central components of the protein export machinery of *E. coli* [16], it is currently not possible to image individual peptides bound to fluid lipid bilayers due to their rapid lateral diffusion [11]. Owing to similarity in size, one may expect a small polypeptide chain to diffuse at a rate similar to that of the lipid to which it is bound. A

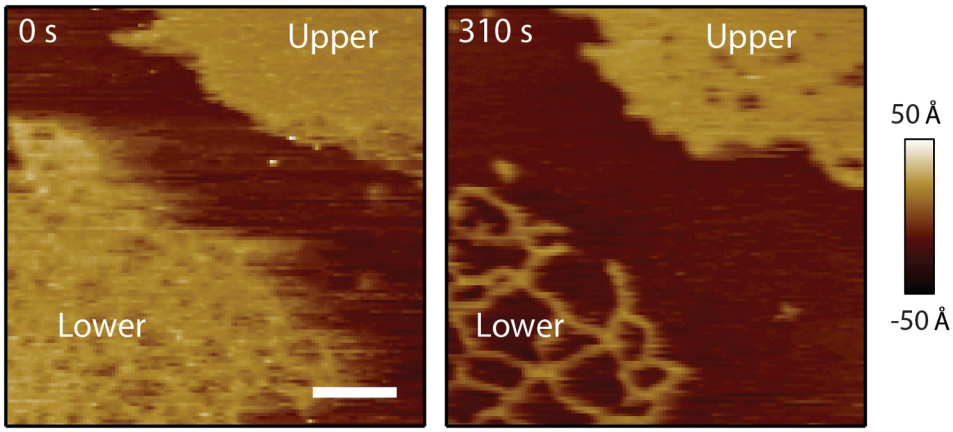

Fig. 2. Neighboring lipid bilayer patches exhibit different stages of remodeling. Upper and lower DOPC lipid patches are identified, separated by a small distance (~150 nm). Though both patches are subject to the same concentration of BaxE5 they behave quite differently. In particular, the upper patch is only beginning to exhibit pore-like voids at 310 s, whereas the lower patch is completely disrupted. The scale bar is 100 nm. Data adapted from ref [7].

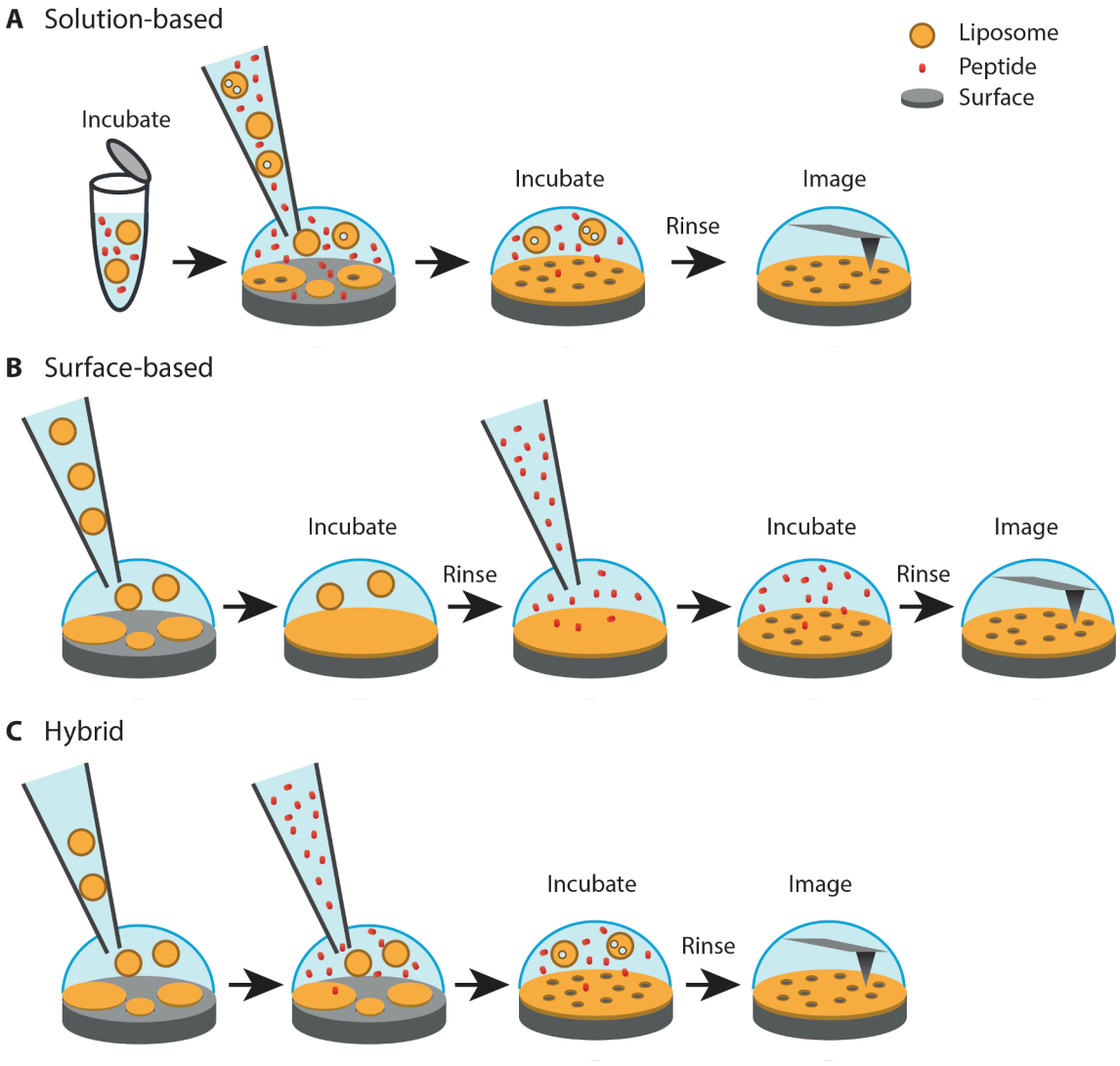

Fig. 3. Cartoons depicting different sample preparation methods. (A) In a solution-based method, the peptide and liposomes are incubated together in an Eppendorf tube prior to deposition onto a clean flat surface. After surface incubation, the sample is rinsed and imaged. Pores are drawn as circular defects in liposomes and surface supported bilayers. (B) Surface-based incubation method where bare liposomes form a supported lipid bilayer. Peptides are then added to the preformed bilayer, incubated, rinsed and imaged. (C) Hybrid method in which liposomes are deposited on the surface first. After a short time, peptide is added. Finally, the sample is incubated, rinsed, and imaged.

recent SLB study tracked the lateral motion of individual DOPC molecules in the surface-distal leaflet and extracted a diffusion constant >4 $\mu m^2/s$ at room temperature [45]. Hence, the lipid bilayer remodeling structures that are visualized via AFM (i.e., topographical features that are stable on the timescale of current imaging technology) are likely due to the action of several individual peptides.

2.2.2. Spatial resolution

Spatial resolution is a fundamental factor in any microscopy method. This is especially true when characterizing small (~10 Å) pore-like voids in fluid lipid bilayers. Indeed, this dimension is smaller than the effective radius of the tip (typically, $R_{tip} \sim 80$ Å) employed by many researchers. Images should be taken with a small pixel size (or step size), *px*. Ideally, $px < R_{tip}$, as this will increase precision in measurements of structural properties. AFM images are a convolution of the tip geometry with individual surface features. Resolution is limited by the probe geometry and can also depend on user input parameters. Many AFM tips, including those used in the studies reported here (Olympus biolever mini: $R_{tip} \sim 80$ Å, cone angle ~17.5°) cannot translocate through the entire thickness of a small peptide-induced membrane pore. We note that the biolever mini represents a compromise between tip sharpness and other cantilever attributes (geometry/dimensions, effective mass, stiffness) which influence force control and measurement bandwidth in fluid. Because tips are not infinitely sharp, as pore radius decreases, the amount of the pore accessible to the tip also decreases. These effects are simulated in Fig. 4 and discussed in Section 3.3.1.

2.2.3. Temporal resolution

Time resolution is another important aspect of AFM imaging [28,29,46,47]. Collecting a series of images of a single area allows observation of dynamics in the lipid remodeling behavior. For example, Fig. 5A displays a series of images of BaxE5 induced poration in a DOPC bilayer at acidic pH [7]. This peptide was derived from Bax, a protein that is known to disrupt the mitochondrial outer membrane [48]. The series of images show dynamics of a single pore-like feature undergoing conformational changes over 420 s. To further increase time resolution, high speed AFM imaging technology can be employed [17,47]. Alternatively, the slow scan axis of a conventional AFM can be disabled to capture kymographs. These are one dimensional line scans over a single feature in time (neglecting the effects of tip/sample drift). Depending on

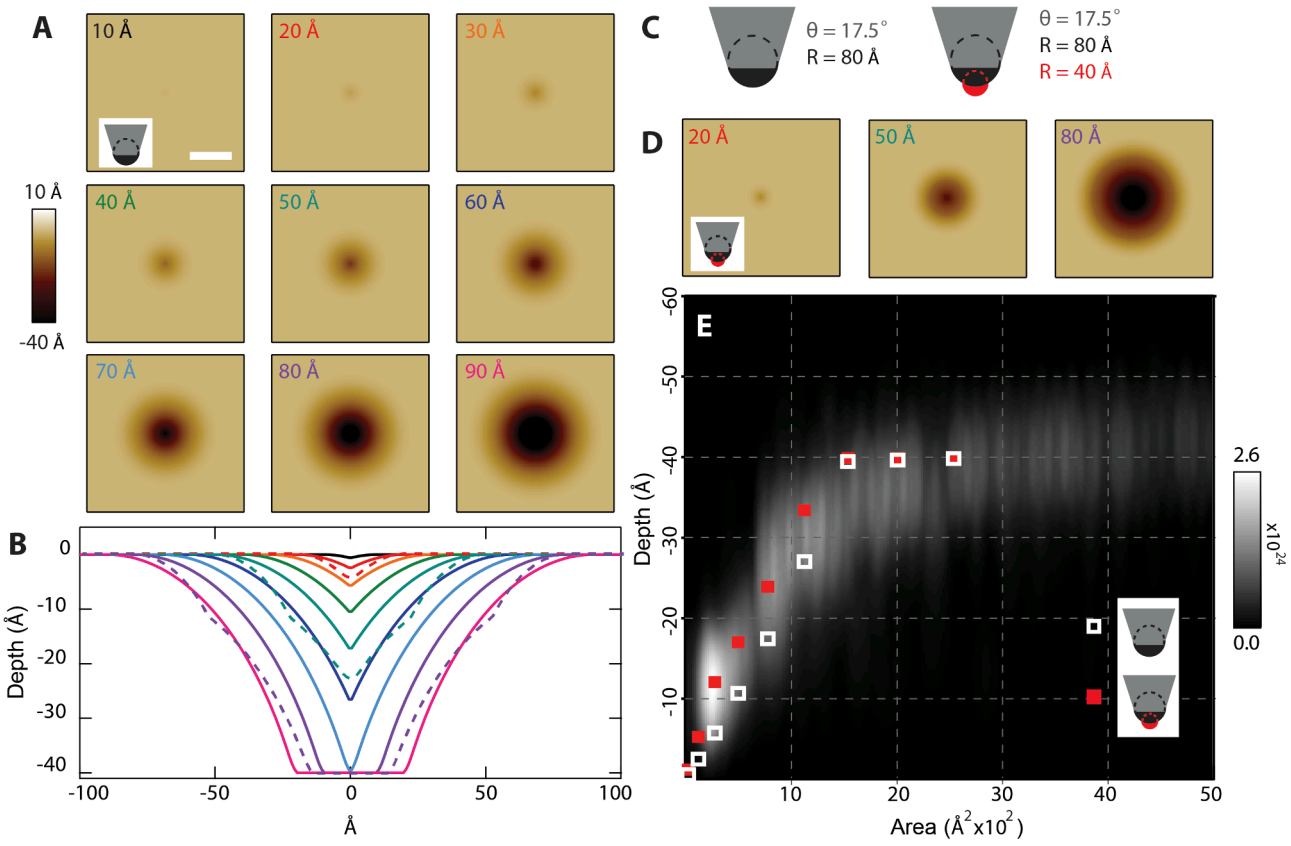

Fig. 4. Simulated AFM images of pores and comparison to experimental data. Simulated images are generated as a convolution of a cylindrical pore structure and an assumed AFM tip geometry. (A) Images simulated from pores of increasing radii (indicated in the upper left corner of each panel). The pore depth was held constant at 40 Å, characteristic of the lipid bilayer thickness. The tip geometry was approximated as a cone (angle $\theta = 17.5$) truncated with a sphere of radius 80 Å, sketched in panel (C, *left*). The lateral scale bar in the first image is 50 Å and applies to all images. (B) Line scans (color coded by pore radius) through the center of each simulated pore are plotted showing the profile of each pore. Note, the tip reaches the bottom of the lower bilayer leaflet only for pores exhibiting radii ≥70 Å. (C, *right*) In an alternative tip geometry, a smaller, overlapping hemisphere of radius 40 Å is added to the tip apex. (D) Three pores simulated with this alternative tip geometry. Line scans through these pores are overlaid in panel B, *dashed*. (E) A 2D smoothed histogram showing pore depth versus pore area for experimental data of the peptide pHD108 with POPC [28]. The probability density is shown in grayscale and is normalized to unity when the ordinate and abscissa are plotted in MKS units. Simulation results (*squares*) show that the small hemispherical tip modification (*red*) increases the accuracy of the simulated images. (For interpretation of the references to color in this figure legend, the reader is referred to the web version of this article.)

the scan rate, this can push topographical measurements into the millisecond regime. An example of a kymograph for pore-like features formed by the pHD108 peptide in a POPC bilayer at acidic pH is shown in Fig. 5B [28]. This peptide was synthetically evolved from melittin to disrupt membranes under acidic conditions at low concentration [49]. Variations from line to line show significant changes in pore depth and radius on a <500 ms timescale (320 ms per line).

2.2.4. Statistical weight of a data set

Large scale imaging increases the statistical weight of the dataset and provides a more accurate picture of ensemble behavior. Qualitatively, lipid bilayer remodeling trends should be reproducible in day-to-day measurements. There are also quantitative methods to check the statistical relevance of image data. A method commonly used in statistical inference is bootstrapping, in which a so-called "bootstrapped" data set is created from the original set by deleting points and replacing them with resampled points [50]. Comparison of certain statistical metrics (such as mean, median, skewness, etc.) or analyzing the distribution of these metrics for a large number of bootstrapped datasets allows unbiased judgement as to whether enough data has been gathered to accurately represent the behavior of the system [51].

2.2.5. Artifacts

Geometric and/or chemical properties of the tip apex can change during imaging, leading to artifacts including double imaging or shadowing [42]. This occurs frequently if there is loosely adsorbed material available to bind to the tip during imaging. Though minimized by rinsing, one has to be constantly on the lookout for such artifacts and clean or change the tip when necessary. We typically clean tips via alternated rinsing in ethanol followed by milli-Q water from squirt bottles, then blowing dry using ultrapure nitrogen. Additionally, an oxygen plasma apparatus (Harrick Plasma, PDC-001) can be used to remove carbonaceous material from the tip.

2.3. Verifying the presence of a lipid bilayer

A fundamental requirement to study peptide-induced lipid bilayer remodeling is to ensure that a supported lipid bilayer is present in the region of interest of the sample. Conveniently, in the case of pore-forming peptides under appropriate conditions, the remodeling itself is evidence of the lipid bilayer. Methods to verify the presence of a bilayer are only necessary when trouble shooting, for example, if no remodeling behavior is observed, or when carrying out control experiments in which only lipid is present.

Several AFM-based methods can be employed for bilayer verification. The first and most straightforward is to locate the edge of a bilayer patch in an AFM image. The topographical height of a lipid bilayer is typically 4–5 nm [52]. However, in some cases, the bilayer spreads

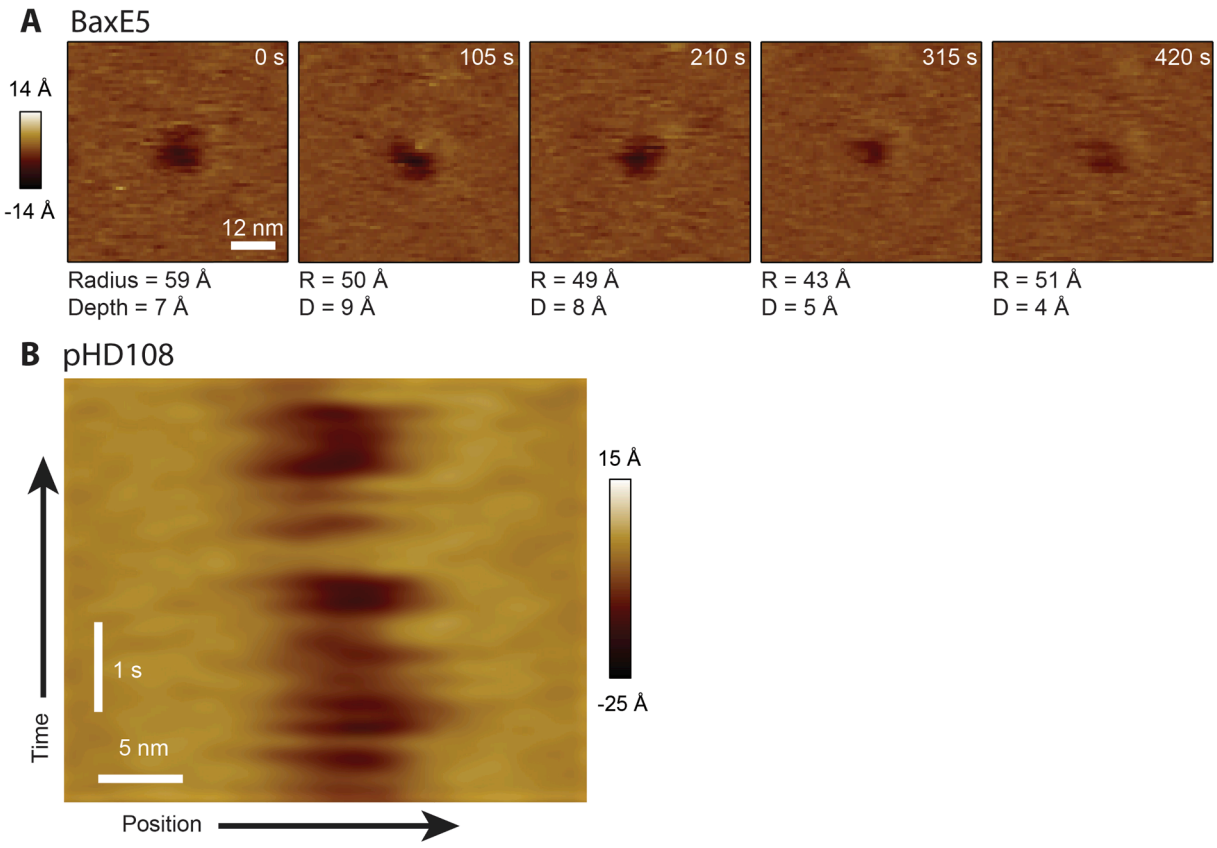

Fig. 5. (A) A series of images of a single BaxE5 pore showing structural changes over time. Hessian blob analysis of each image yields measurements of radius and depth, displayed below the image. Data adapted from ref [7]. Panel B is an example of a kymograph of an individual pHD108 pore, with position on the x-axis and time on the y-axis. The width and depth of the pore vary significantly from line to line, which were acquired at 320 ms intervals. The pore appears to briefly disappear halfway up the kymograph, then reappear. Data adapted from ref [28].

completely, leaving no patches or edges to measure. Comparing AFM-measured surface roughness with and without lipid is one method to verify its existence in such cases; however, this metric is dependent on tip geometry and imaging parameters. Hence these measurements have to be performed with the same exact tip and performed with care [43]. Analysis of force-distance curves in lipid bilayer rupture measurements provides another method to demonstrate a supported lipid bilayer [53,54]. However, large forces are usually required (>1 nN) to generate lipid breakthrough events. Such high forces can also break covalent bonds [55] leading to irreversible tip damage and lipid or other contamination on the tip. In addition to AFM, optical methods can be used to verify the presence of lipid bilayers over large length scales, but these techniques generally require the addition of fluorophores [56,57]. Some advanced optical techniques do not require labeling and hence are natural complements to AFM measurements [58,59].

2.4. Colocalization of membrane remodeling modes

Peptide-induced pore formation has been shown to be affected by a number of factors, such as incubation time, peptide-to-lipid molar ratio, lipid species, and the pH of the environment [26–28]. All of these factors can be investigated in a bulk biochemical manner; however, AFM imaging offers unique visualization that can discriminate between remodeling modes and determine if they are colocalized on the bilayer.

Figs. 1 & 7 illustrate distinct pore-like voids and other lipid bilayer remodeling modes. The images of MelP5, a peptide synthetically evolved from melittin to form large and stable pores at low concentration in zwitterionic lipid [60], with POPC (Fig. 1A & B and Fig. 7) unveil interesting aspects that are likely related to the pore-forming mechanism [27]. At low P:L (Fig. 1A and Fig. 7) punctate pore-like voids were found to co-localize with thinned areas of the membrane, consistent with a two-step pore-formation process dependent on local peptide concentration [61]. For this system, AFM imaging shed light on phenomena accompanying membrane poration that would be challenging if not impossible to observe using other methods. At a higher P:L value (Fig. 1B), larger scale linear features or trenches were observed, possibly resulting from coalescing of several pore-like voids.

2.5. Imaging in acidic conditions

Lipid bilayer remodeling emanating from pH-dependent peptides must be studied in a carefully controlled environment. Many pH-dependent peptides are designed to be activated in acidic conditions [1,7,28,62] and many commercial AFM tools are capable of operating in low pH environments. Fig. 1C & D shows lipid bilayer remodeling by a pH-dependent peptide derived from melittin, pHD108, at two P:L values [28]. Here, the peptide was incubated with POPC lipid using the solution-based incubation method (Fig. 3A) in a pH 4.0 buffer. An approximately 25% increase in the peptide concentration resulted in a significant increase in the number of pore-like voids per unit area (compare Fig. 1C and 1D). These results highlight the significant role that the P:L can play in the remodeling behavior. That said, defining the P:L during an AFM experiment with much precision is challenging (discussed in Section 2.1.2). Additionally we note that varying pH throughout the course of an AFM imaging session can be challenging due to interfacial hydrodynamics. No slip boundary conditions limit fluid flow at or very near surfaces [63].

2.6. Control experiments

Control experiments add to the broad picture of AFM imaging data and can reinforce validity of the conclusions. Controls can include studying the individual components of the peptide-lipid system in nominally identical conditions. For example, in low-pH studies, the bare lipid membrane should be characterized under the same acidic conditions for comparison to the peptide-lipid sample. Imaging peptide without lipid can also give insights into the initial steps of the membrane disruption process. Such measurements can potentially be used to evaluate peptide oligomerization or aggregation in solution prior to any membrane interactions.

3. Analysis of AFM image data

3.1. Region of interest detection

Images of membrane remodeling can be analyzed using a variety of particle-detection algorithms. In the King Lab, we have used both traditional height-thresholds and the newly introduced Hessian blob detection algorithm [64]. There are benefits and drawbacks to each of these methods, which will be described.

A traditional particle detection method utilizes a height threshold set at a user specified background level. Any features with heights either above or below this background limit are isolated as regions of interest. Pixels from these regions are extracted and used for further analysis. Creating a histogram of pixel values yields a distribution of depths for pore-like features. Footprint area is another valuable parameter to analyze. While the height thresholding method may be able to define a pore perimeter close to the pore edge, it is sensitive to user input and requires a high amount of preprocessing. Minimizing user input bias in data analysis is key to achieve an objective interpretation. Furthermore, when processing large quantities of data for statistical analyses, the requirement of user input becomes increasingly time consuming.

The Hessian blob algorithm (described in detail elsewhere [64]) is a particle detection software that does not necessitate a large amount of preprocessing or user input. Briefly, the algorithm automatically detects individual point-like features or particles within an image and then precisely defines particle perimeters using a method from differential geometry. One potential drawback of this method is the slight underestimation of footprint area due to a feature perimeter defined using Gaussian curvature. However, this is a systemic error that can be quantified, e.g., through simulations. We note that even if left uncorrected, the relative difference between footprint area populations should remain accurate.

3.2. Statistical data interpretation

Once features of interest such as pore-like voids or membrane-thinned regions have been extracted from image data, populations can be identified and separated by fitting histograms with a summation of model distributions (e.g., Gaussians). In general, increasing the number of distributions increases the accuracy of the fit. How does one know when to stop adding additional distributions? Doing so in an unbiased manner requires some penalty for overfitting. Several criteria have been developed for the purpose of model selection. Here, we use the Bayesian information criterion (*BIC*) to penalize overfitting and optimize the number of model distributions needed for a given histogram of interest, such as a pore area distribution. The *BIC* for a model is given by

$$BIC = k\ln n - 2\ln\left(\widehat{L}\right)$$

Where, k is the number of free parameters in the model, n is the number of points in the data set being fitted, and $\widehat{L}$ is the maximized likelihood function for the fitted model [65]. Note that k will scale with the number of model distributions (e.g., Gaussians) added. As a specific example of this method, Fig. 6 shows an area histogram fitted with N Gaussian distributions for pore-like features formed by the peptide Candidalysin in a DOPC membrane. *BIC*s are computed for the summations of N Gaussian distributions. The minimum *BIC* in the plot (Fig. 6B) gives the optimal number of distributions to use when fitting the histogram, in this case, $N = 2$ (Fig. 6A). In this way the number of distinct populations of pore-like voids can be determined in a statistically robust and unbiased method.

3.3. Challenges of demonstrating bona fide transmembrane pores via AFM

In an AFM image, transmembrane pores appear as highly localized voids in the membrane. However, many pores have radii smaller than the effective radius of the apex of the AFM tip itself. Despite this complication, pore-like features can be distinguished based on footprint area. For example, in Fig. 6 Bayesian model-selection was used to

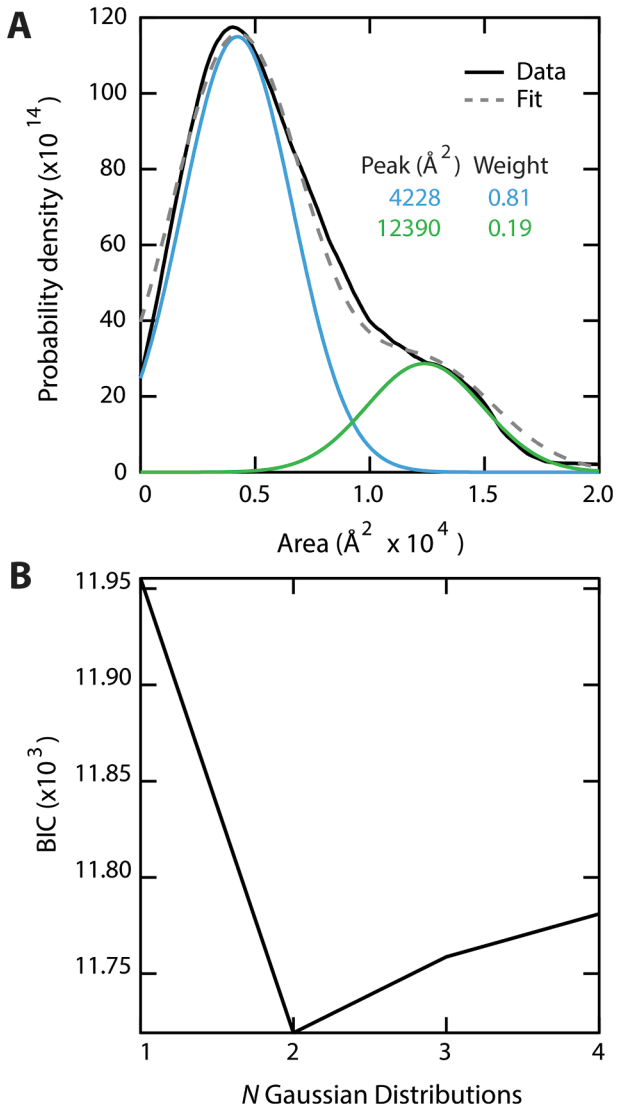

Fig. 6. Bayesian information criterion provides unbiased modeling by preventing overfitting. A model is selected and fitted to the smoothed area histogram of $N = 601$ pores formed by the peptide Candidalysin in DOPC using BIC analysis. (A) Two Gaussian distributions are fitted to the area histogram based on a minimized BIC calculation. The peak position and weight (calculated from the area under each curve) of each distribution are also displayed. The probability density is normalized to unity when plotted in MKS units. (B) BICs are plotted for N Gaussian distributions, revealing a minimum at $N = 2$.

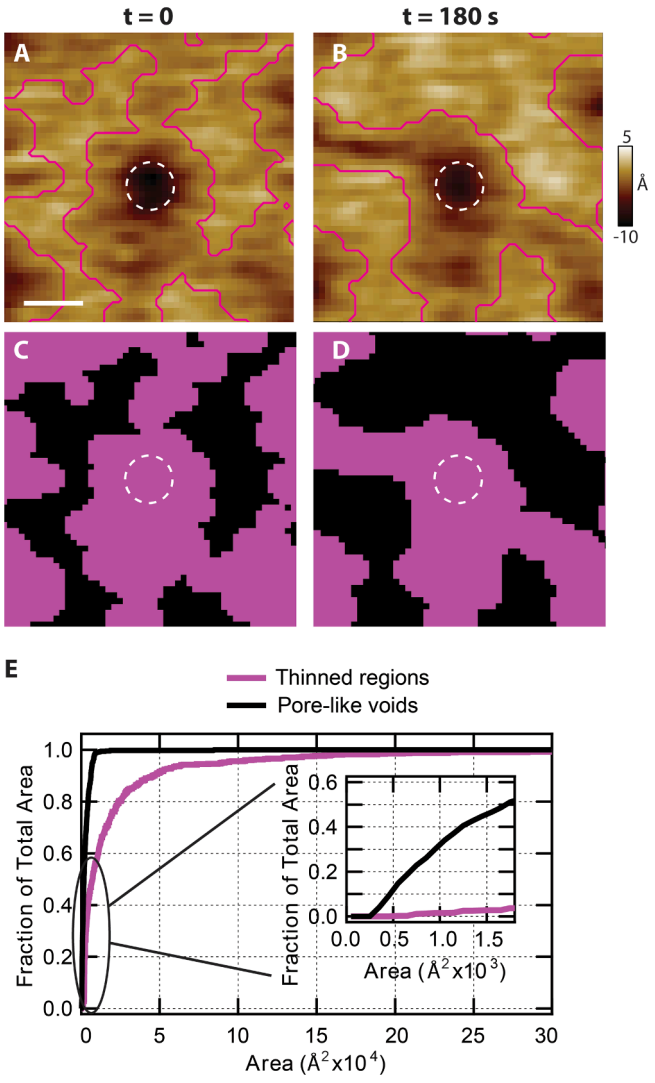

Fig. 7. Discriminating membrane-thinned regions from pore-like voids. (A & B) Membrane-thinned regions show significant topographical changes in sequential images of MelP5 remodeling POPC. A relatively static pore-like void (*dashed circle*) is observed in the center of both images. A dilated mask (*magenta contour*) guides the eye in delineating the boundary between membrane-thinned and topographically higher regions. A few pixels are left out of the masked region due to dilation. The time dependence of this boundary in A & B is highlighted (C & D, respectively). Here membrane-thinned regions are purple, topographically higher regions are black. The lateral scale bar shown in A is 10 nm and applies to all panels. (E) Integrated area histograms for pore-like features ($N = 572$, *black*) and the thinned regions ($N = 710$, *purple*). *Inset:* Detailed view highlights differences between the two populations. Data adapted from ref [27]. (For interpretation of the references to color in this figure legend, the reader is referred to the web version of this article.)

separate populations with peak positions at 4228 Å^2 and 12,390 Å^2. If these features are assumed to be circular, the radii of these peak positions are 37 Å and 63 Å, respectively, both less than the nominal tip radius (~80 Å). Due to convolution of tip geometry with the membrane topography, artificially shallow depths are expected. Additionally, one would expect that these depths scale with the radius of the pore, as shown in simulated AFM images and experimental pHD108 data (Fig. 4).

3.3.1. Depth versus radius analysis

The close connection between AFM-measured depth and feature radius has been observed experimentally and can provide evidence of bona fide transmembrane pores. Simulated images show the dependence of AFM-measured pore depth on the radius of the pore and on the shape of the AFM tip apex. Simulations are calculated as a morphological dilation of an assumed pore geometry and tip geometry [16,18]. In Fig. 4, the tip is first modeled as a cone truncated to a single hemispherical endcap (radius = 80 Å, cone angle = 17.5). This is the nominal geometry of the tip apex supplied by the manufacturer (Olympus, Biolever mini). The membrane and pore are modeled as a plane with a cylindrical through-hole. The radius of the simulated pore is varied between 10 Å and 90 Å with a step size of 10 Å (Fig. 4A). The pore depth is kept constant at 40 Å, transecting the lipid bilayer in a rectilinear fashion. The solid lines in Fig. 4B show line scans through the center of each simulated image (color coded by pore radius). Each line scan shows a profile of the convolved pore and shows the relationship between pore radius and the AFM-measured depth, based on the assumed tip geometry. As the pore radius decreases, so too does the AFM-measured depth.

Better agreement between simulations and experiments can be achieved by assuming a sharper tip than nominal dimensions, which tend to be conservative. In an alternative tip geometry, a smaller hemisphere (radius = 40 Å) is added to the nominal tip apex such that it overlaps the larger hemispherical endcap (radius = 80 Å). The geometry of this alternative tip is drawn next to the nominal tip (Fig. 4C). Three simulated AFM images of pores (radii: 20, 50, and 80 Å, respectively) are shown using this alternative tip geometry (Fig. 4D). Line scans through these three pores are overlaid (Fig. 4B, *dashed*) and can be compared to those of the same size pores with the nominal tip geometry. A bivariate smoothed histogram showing experimentally measured pore depth versus pore area for the pHD108 peptide with POPC imaged at pH 4 is also shown (Fig. 4E) [28]. Simulation data are overlaid as squares on the experimental data. The results indicate that the alternative tip geometry (*red squares*) increases the accuracy of the simulations compared to the nominal tip geometry (*white squares*). More generally, the overall agreement between experimental data and simulations implies that the geometrical metrics extracted from the experimental AFM images are limited by tip geometry. Many features appear as sharp as the tip itself. Such highly localized voids in the bilayer are likely to be pores.

3.3.2. Differential mobility of remodeling modes

Studying the lateral mobility of topographic features identified on a lipid bilayer surface can be used to discriminate between distinct remodeling modes and can provide further evidence of pores. By definition, a transmembrane pore penetrates both the upper and lower bilayer leaflets. During AFM imaging, the lower bilayer leaflet is in close proximity (~10 Å [66,67]) to the solid-state supporting surface. This proximity suppresses diffusion of lipid molecules in the surface-proximal leaflet substantially more than lipids in the surface-distal leaflet [45,68]. Hence, a bona fide pore would experience greater drag force due to its direct coupling with the surface-proximal leaflet. On the other hand, non-transmembrane features accessible to the AFM tip would not be strongly coupled to the surface-proximal leaflet. As a consequence, one would expect non-transmembrane features to exhibit more lateral motion per unit time than pores. To demonstrate this we compared dynamics of membrane-thinned regions to pore-like features generated in supported POPC bilayers exposed to MelP5. The results show that the distinct membrane remodeling modes exhibit different lateral mobilities (Fig. 7A–D). In particular, significant topographical changes of the membrane thinned region were apparent whereas the pore-like void was much more stable. The areal extent of the membrane-thinned region increased by 30% on the 180 s timescale shown in Fig. 7. Taken together, these observations with POPC and MelP5 are consistent with the assertions that (*i*) the membrane thinned regions do not penetrate into the surface proximal leaflet and that (*ii*) the pore-like voids are indeed transmembrane pores.

3.3.3. Footprint area analysis

A challenge is to distinguish between a pore, a thinned area of the

membrane, and a lipid defect caused when bilayer coverage is interrupted. A defining feature of a pore is that it is small, usually exhibiting radii less than the nominal tip radius. Additionally, one may expect pores to exhibit specific structures corresponding to minima in a complex energy landscape. Hence, when analyzed statistically, pores of a specific structure should have a very narrow distribution of footprint area. In contrast, membrane-thinned regions can often come about from peptides that are bound to the membrane with their long axis oriented parallel to the membrane surface [61]. Due to a lack of underlying structure, membrane-thinned regions as well as lipid bilayer defects should exhibit a broad array of footprint areas. For example, $N = 710$ thinned regions of the POPC were delineated algorithmically from a series of images of MelP5 remodeling, as were $N = 572$ pore-like voids [27]. Integrated area histograms of both populations were compiled and plotted (Fig. 7E). For pore-like voids, the integral saturated to unity quickly. This indicates that the majority of footprint areas are localized into a well-defined peak. However, for the membrane-thinned regions, the integral did not reach unity nearly as rapidly, owing to a lack of underlying structure. Additionally, for each image there was on average 59 membrane-thinned features that accounted for 37% of the total area of the image. Concurrently there were 190 pore-like voids that accounted for only 3% of the total area of the image. The membrane-thinned regions were therefore substantially larger than the pore-like voids.

Taken together, these observations provide additional evidence that the highly localized pore-like voids identified in MelP5 are likely to be bona fide transmembrane pores. At the same time, the membrane-thinned regions exhibited a broad area distribution with no well-defined peak in the histogram. This is a good indication that there is no underlying structure; hence, membrane thinned features are not likely to be pores.

3.3.4. *Corroboration with other techniques*

Like many experimental approaches, AFM analysis is most powerful when combined with other techniques. Agreement between independent lines of inquiry provides further confidence in the identification of transmembrane pores and in their overall structural characterization. A variety of functional assays can be performed side-by-side with AFM imaging. For example, leakage experiments are a common bulk measurement that can verify the presence of transmembrane pores or large membrane defects [1]. By varying the size of the molecules used in leakage assays, the method can also provide insight into the pore radius and the results can be compared to AFM measurements [27,28].

4. Conclusion and outlook

In its applications to biomolecules, the atomic force microscope has proven to be a powerful tool in characterization of structure and dynamics. Its ability to directly visualize biological systems in fluid at a single molecule level gives insight into heterogeneity, asynchronous behavior, and structural changes that would be difficult or impossible to resolve otherwise. Our group has utilized this ability to study pore-forming peptides in a planar lipid bilayer environment.

In this work we presented an overview of methodology used to achieve high precision AFM data on membrane-peptide samples. We discussed optimizing imaging conditions through careful sample preparation, control of imaging parameters, and awareness of artifacts. Additionally, we presented analysis methods that reduce user bias and characterized remodeling modes in a robust statistical manner. Tip-geometry constraints on AFM images give rise to shallow pores with depths smaller than the thickness of a lipid bilayer. This makes it challenging to unambiguously identify pores in AFM images. Several methods were presented to increase confidence in discriminating between transmembrane pores, membrane defects and membrane-thinned regions.

Technical advances on the horizon could improve data quality. Advanced lithographic methods including ice lithography [69,70] could improve spatial resolution by enabling precise control over AFM tip apex geometry and chemical species. Advancements in AFM time resolution will allow observation of pore evolution on increasingly short timescales. The effective mass and cross-sectional area of commercial AFM tips can be modified and fine-tuned using focused ion beam milling to reduce mechanical response times in fluid [15,71]. One of the unique benefits of single molecule investigations is that they can be combined to address the same system at the same moment in time. For example, single channel recording can potentially be performed simultaneously with AFM imaging of pore forming peptides at work. Reduction of ionic current passing through the membrane while the tip passes over a pore-like feature could unambiguously identify that feature as a transmembrane pore, as has been shown with solid state nanopores [72]. We think that it is fair to conclude that AFM has a bright future for improving understanding of peptide-induced lipid bilayer remodeling.

Declaration of Competing Interest

The authors declare that they have no known competing financial interests or personal relationships that could have appeared to influence the work reported in this paper.

Acknowledgements

This work was supported by the National Science Foundation [grant number: 1709792, G.M.K.] and the National Institutes of Health [grant number: R01GM120642, F.N.B].

References

[1] S. Guha, J. Ghimire, E. Wu, W.C. Wimley, Mechanistic landscape of membrane-permeabilizing peptides, Chem. Rev. 119 (9) (2019) 6040–6085.
[2] H. El-Seedi, A. Abd El-Wahed, N. Yosri, S.G. Musharraf, L. Chen, M. Moustafa, X. Zou, S. Al-Mousawi, Z. Guo, A. Khatib, S. Khalifa, Antimicrobial properties of Apis mellifera's bee venom, Toxins (Basel) 12 (7) (2020).
[3] D.L. Moyes, D. Wilson, J.P. Richardson, S. Mogavero, S.X. Tang, J. Wernecke, S. Hofs, R.L. Gratacap, J. Robbins, M. Runglall, C. Murciano, M. Blagojevic, S. Thavaraj, T.M. Forster, B. Hebecker, L. Kasper, G. Vizcay, S.I. Iancu, N. Kichik, A. Hader, O. Kurzai, T. Luo, T. Kruger, O. Kniemeyer, E. Cota, O. Bader, R. T. Wheeler, T. Gutsmann, B. Hube, J.R. Naglik, Candidalysin is a fungal peptide toxin critical for mucosal infection, Nature 532 (7597) (2016) 64-+.
[4] Y. Shai, Z. Oren, From "carpet" mechanism to de-novo designed diastereomeric cell-selective antimicrobial peptides, Peptides 22 (10) (2001) 1629–1641.
[5] K. Hristova, C.E. Dempsey, S.H. White, Structure, location, and lipid perturbations of melittin at the membrane interface, Biophys. J . 80 (2) (2001) 801–811.
[6] K. El Kirat, Y.F. Dufrene, L. Lins, R. Brasseur, The SIV tilted peptide induces cylindrical reverse micelles in supported lipid bilayers, Biochemistry-Us 45 (30) (2006) 9336–9341.
[7] K.G. Schaefer, B. Grau, N. Moore, I. Mingarro, G.M. King, F.N. Barrera, Controllable membrane remodeling by a modified fragment of the apoptotic protein Bax, Faraday Discuss. (2020), https://doi.org/10.1039/D0FD00070A.
[8] M. Utjesanovic, T.R. Matin, K.P. Sigdel, G.M. King, I. Kosztin, Multiple stochastic pathways in forced peptide-lipid membrane detachment, Sci. Rep. 9 (1) (2019) 451.
[9] T.R. Matin, K.P. Sigdel, M. Utjesanovic, B.P. Marsh, F. Gallazzi, V.F. Smith, I. Kosztin, G.M. King, Single-molecule peptide-lipid affinity assay reveals interplay between solution structure and partitioning, Langmuir 33 (16) (2017) 4057–4065.
[10] S. Morandat, S. Azouzi, E. Beauvais, A. Mastouri, K. El Kirat, Atomic force microscopy of model lipid membranes, Anal. Bioanal. Chem. 405 (5) (2013) 1445–1461.
[11] K. Hammond, M.G. Ryadnov, B.W. Hoogenboom, Atomic force microscopy to elucidate how peptides disrupt membranes, Biochim. Biophys. Acta, Biomembr. (2020), 183447.
[12] G. Binnig, C.F. Quate, C. Gerber, Atomic force microscope, Phys. Rev. Lett. 56 (9) (1986) 930–933.
[13] C.A. Bippes, D.J. Muller, High-resolution atomic force microscopy and spectroscopy of native membrane proteins, Rep. Prog. Phys. 74 (8) (2011).
[14] T. Fukuma, K. Kobayashi, K. Matsushige, H. Yamada, True atomic resolution in liquid by frequency-modulation atomic force microscopy, Appl. Phys. Lett. 87 (3) (2005).
[15] D.T. Edwards, J.K. Faulk, A.W. Sanders, M.S. Bull, R. Walder, M.-A. LeBlanc, M. C. Sousa, T.T. Perkins, Optimizing 1-mus-resolution single-molecule force spectroscopy on a commercial atomic force microscope, Nano Lett. 15 (10) (2015) 7091–7098.

[16] R.R. Sanganna Gari, K. Chattrakun, B.P. Marsh, C. Mao, N. Chada, L.L. Randall, G. M. King, Direct visualization of the E. coli Sec translocase engaging precursor proteins in lipid bilayers, Sci. Adv. 5 (6) (2019) eaav9404.
[17] K.P. Sigdel, L.A. Wilt, B.P. Marsh, A.G. Roberts, G.M. King, The conformation and dynamics of P-glycoprotein in a lipid bilayer investigated by atomic force microscopy, Biochem. Pharmacol. 156 (2018) 302–311.
[18] N. Chada, K. Chattrakun, B.P. Marsh, C. Mao, P. Bariya, G.M. King, Single-molecule observation of nucleotide induced conformational changes in basal SecA-ATP hydrolysis, Sci. Adv. 4 (10) (2018) eaat8797.
[19] K. El Kirat, S. Morandat, Y.F. Dufrene, Nanoscale analysis of supported lipid bilayers using atomic force microscopy, Bba-Biomembranes 1798 (4) (2010) 750–765.
[20] A.L. Weisenhorn, F.J. Schmitt, W. Knoll, P.K. Hansma, Streptavidin binding observed with an atomic force microscope, Ultramicroscopy 42–44 (Pt B) (1992) 1125–1132.
[21] H.A. Rinia, M.M.E. Snel, J.P.J.M. van der Eerden, B. de Kruijff, Visualizing detergent resistant domains in model membranes with atomic force microscopy, FEBS Lett. 501 (1) (2001) 92–96.
[22] H.A. Rinia, B. de Kruijff, Imaging domains in model membranes with atomic force microscopy, FEBS Lett. 504 (3) (2001) 194–199.
[23] M. Meincken, D.L. Holroyd, M. Rautenbach, Atomic force microscopy study of the effect of antimicrobial peptides on the cell envelope of Escherichia coli, Antimicrob. Agents Chemother. 49 (10) (2005) 4085–4092.
[24] L. Connelly, H. Jang, F.T. Arce, R. Capone, S.A. Kotler, S. Ramachandran, B. L. Kagan, R. Nussinov, R. Lal, Atomic force microscopy and MD simulations reveal pore-like structures of all-D-enantiomer of Alzheimer's beta-amyloid peptide: relevance to the ion channel mechanism of AD pathology, J. Phys. Chem. B 116 (5) (2012) 1728–1735.
[25] H. Lin, R. Bhatia, R. Lal, Amyloid beta protein forms ion channels: implications for Alzheimer's disease pathophysiology, FASEB J. 15 (13) (2001) 2433–2444.
[26] J. Pan, N.K. Khadka, Kinetic defects induced by melittin in model lipid membranes: a solution atomic force microscopy study, J. Phys. Chem. B 120 (20) (2016) 4625–4634.
[27] A.E. Pittman, B.P. Marsh, G.M. King, Conformations and dynamic transitions of a melittin derivative that forms macromolecule-sized pores in lipid bilayers, Langmuir 34 (28) (2018) 8393–8399.
[28] S.Y. Kim, A.E. Pittman, E. Zapata-Mercado, G.M. King, W.C. Wimley, K. Hristova, Mechanism of action of peptides that cause the ph-triggered macromolecular poration of lipid bilayers, J. Am. Chem. Soc. 141 (16) (2019) 6706–6718.
[29] T.K. Lind, P. Zielinska, H.P. Wacklin, Z. Urbanczyk-Lipkowska, M. Cardenas, Continuous flow atomic force microscopy imaging reveals fluidity and time-dependent interactions of antimicrobial dendrimer with model lipid membranes, ACS Nano 8 (1) (2014) 396–408.
[30] D.J. Muller, D. Fotiadis, S. Scheuring, S.A. Muller, A. Engel, Electrostatically balanced subnanometer imaging of biological specimens by atomic force microscope, Biophys. J. 76 (2) (1999) 1101–1111.
[31] J.N. Israelachvili, Intermolecular and Surface Forces, 3rd ed., Academic Press, 2011.
[32] H. Raghuraman, A. Chattopadhyay, Effect of ionic strength on folding and aggregation of the hemolytic peptide melittin in solution, Biopolymers 83 (2) (2006) 111–121.
[33] D.S. Alves, J.M. Westerfield, X.J. Shi, V.P. Nguyen, K.M. Stefanski, K.R. Booth, S. Kim, J. Morrell-Falvey, B.C. Wang, S.M. Abel, A.W. Smith, F.N. Barrera, A novel pH-dependent membrane peptide that binds to EphA2 and inhibits cell migration, Elife 7 (2018).
[34] V.P. Nguyen, D.S. Alves, H.L. Scott, F.L. Davis, F.N. Barrera, A novel soluble peptide with ph-responsive membrane insertion, Biochemistry-Us 54 (43) (2015) 6567–6575.
[35] O.G. Mouritsen, Life – As a Matter of Fat, Springer-Verlag, Berlin, 2005.
[36] W.C. Wimley, S.H. White, Experimentally determined hydrophobicity scale for proteins at membrane interfaces, Nat. Struct. Biol. 3 (10) (1996) 842–848.
[37] L.K. Tamm, H.M. McConnell, Supported phospholipid bilayers, Biophys. J. 47 (1) (1985) 105–113.
[38] T.R. Matin, M. Utjesanovic, K.P. Sigdel, V.F. Smith, I. Kosztin, G.M. King, Characterizing the locus of a peripheral membrane protein-lipid bilayer interaction underlying protein export activity in E. coli, Langmuir 36 (8) (2020) 2143–2152.
[39] R.P. Richter, R. Berat, A.R. Brisson, Formation of solid-supported lipid bilayers: an integrated view, Langmuir 22 (8) (2006) 3497–3505.
[40] J.A. Jackman, V.V. Costa, S. Park, A. Real, J.H. Park, P.L. Cardozo, A.R. Ferhan, I. G. Olmo, T.P. Moreira, J.L. Bambirra, V.F. Queiroz, C.M. Queiroz-Junior, G. Foureaux, D.G. Souza, F.M. Ribeiro, B.K. Yoon, E. Wynendaele, B. De Spiegeleer, M.M. Teixeira, N.J. Cho, Therapeutic treatment of Zika virus infection using a brain-penetrating antiviral peptide, Nat. Mater. 17 (11) (2018) 971–977.
[41] B. Berne, R. Pecora, Dynamic Light Scattering: With Applications to Chemistry, Biology, and Physics, John Wiley and Sons, New York, 1976.
[42] Ricci, D.; Braga, P. C., Recognizing and Avoiding Artifacts in AFM Imaging. In: Braga P.C., Ricci D. (eds) Atomic Force Microscopy. Methods in Molecular Biology. Humana Press: 2004.
[43] N. Chada, K.P. Sigdel, R.R. Gari, T.R. Matin, L.L. Randall, G.M. King, Glass is a viable substrate for precision force microscopy of membrane proteins, Sci. Rep. 5 (2015) 12550.
[44] P.R. Heenan, T.T. Perkins, Imaging DNA equilibrated onto mica in liquid using biochemically relevant deposition conditions, ACS Nano 13 (4) (2019) 4220–4229.
[45] R.L. Schoch, I. Barel, F.L.H. Brown, G. Haran, Lipid diffusion in the distal and proximal leaflets of supported lipid bilayer membranes studied by single particle tracking, J. Chem. Phys. 148 (12) (2018), 123333.
[46] G.E. Fantner, R.J. Barbero, D.S. Gray, A.M. Belcher, Kinetics of antimicrobial peptide activity measured on individual bacterial cells using high-speed atomic force microscopy, Nat. Nanotechnol. 5 (4) (2010) 280–285.
[47] T. Ando, High-speed atomic force microscopy and its future prospects, Biophys. Rev. 10 (2) (2018) 285–292.
[48] K. Cosentino, A.J. Garcia-Saez, Bax and bak pores: are we closing the circle? Trends Cell Biol. 27 (4) (2017) 266–275.
[49] G. Wiedman, S.Y. Kim, E. Zapata-Mercado, W.C. Wimley, K. Hristova, pH-triggered, macromolecule-sized poration of lipid bilayers by synthetically evolved peptides, J. Am. Chem. Soc. 139 (2) (2017) 937–945.
[50] B. Efron, T. Hastie, Computer Age Statistical Inference: Algorithms, Evidence, and Data Science, Cambridge University Press, 2016.
[51] P.H. Nguyen, K.P. Sigdel, K.G. Schaefer, G.A.K. Mensah, G.M. King, A.G. Roberts, The effects of anthracycline drugs on the conformational distribution of mouse P-glycoprotein explains their transport rate differences, Biochem. Pharmacol. 174 (2020), 113813.
[52] D.J. Muller, A. Engel, The height of biomolecules measured with the atomic force microscope depends on electrostatic interactions, Biophys. J. 73 (3) (1997) 1633–1644.
[53] S. Garcia-Manyes, F. Sanz, Nanomechanics of lipid bilayers by force spectroscopy with AFM: a perspective, BBA 1798 (4) (2010) 741–749.
[54] V.O. Saavedra, T.F.D. Fernandes, P.-E. Milhiet, L. Costa, Compression, rupture, and puncture of model membranes at the molecular scale, Langmuir 36 (21) (2020) 5709–5716.
[55] M. Grandbois, M. Beyer, M. Rief, H. Clausen-Schaumann, H.E. Gaub, How strong is a covalent bond? Science 283 (5408) (1999) 1727–1730.
[56] E.T. Castellana, P.S. Cremer, Solid supported lipid bilayers: from biophysical studies to sensor design, Surf. Sci. Rep. 61 (10) (2006) 429–444.
[57] P.S. Cremer, S.G. Boxer, Formation and spreading of lipid bilayers on planar glass supports, J. Phys. Chem. B 103 (13) (1999) 2554–2559.
[58] A.B. Churnside, G.M. King, T.T. Perkins, Label-free optical imaging of membrane patches for atomic force microscopy, Opt. Express 18 (23) (2010) 23924–23932.
[59] J. Andrecka, K.M. Spillane, J. Ortega-Arroyo, P. Kukura, Direct observation and control of supported lipid bilayer formation with interferometric scattering microscopy, ACS Nano 7 (12) (2013) 10662–10670.
[60] G. Wiedman, T. Fuselier, J. He, P.C. Searson, K. Hristova, W.C. Wimley, Highly efficient macromolecule-sized poration of lipid bilayers by a synthetically evolved peptide, J. Am. Chem. Soc. 136 (12) (2014) 4724–4731.
[61] H.W. Huang, Molecular mechanism of antimicrobial peptides: the origin of cooperativity, BBA 1758 (9) (2006) 1292–1302.
[62] W. Li, F. Nicol, F.C. Szoka Jr., GALA: a designed synthetic pH-responsive amphipathic peptide with applications in drug and gene delivery, Adv. Drug Deliv. Rev. 56 (7) (2004) 967–985.
[63] D.J. Acheson, Elementary Fluid Dynamics, Clarendon Press, 1990.
[64] B.P. Marsh, N. Chada, R.R. Sanganna Gari, K.P. Sigdel, G.M. King, The Hessian blob algorithm: precise particle detection in atomic force microscopy imagery, Sci. Rep. 8 (1) (2018) 978.
[65] G. Schwarz, Estimating the dimension of a model, Ann. Statist. 6 (1978) 461–646.
[66] B.W. Koenig, S. Kruger, W.J. Orts, C.F. Majkrzak, N.F. Berk, J.V. Silverton, K. Gawrisch, Neutron reflectivity and atomic force microscopy studies of a lipid bilayer in water adsorbed to the surface of a silicon single crystal, Langmuir 12 (5) (1996) 1343–1350.
[67] K. Chattrakun, D.P. Hoogerheide, C. Mao, L.L. Randall, G.M. King, Protein translocation activity in surface-supported lipid bilayers, Langmuir 35 (37) (2019) 12246–12256.
[68] T. Otosu, S. Yamaguchi, Quantifying the diffusion of lipids in the proximal/distal leaflets of a supported lipid bilayer by two-dimensional fluorescence lifetime correlation spectroscopy, J. Phys. Chem. B 122 (45) (2018) 10315–10319.
[69] A.P. Han, A. Kuan, J. Golovchenko, D. Branton, Nanopatterning on nonplanar and fragile substrates with ice resists, Nano Lett. 12 (2) (2012) 1018–1021.
[70] M. Jaafar, J. Pablo-Navarro, E. Berganza, P. Ares, C. Magen, A. Masseboeuf, C. Gatel, E. Snoeck, J. Gomez-Herrero, J.M. de Teresa, A. Asenjo, Customized MFM probes based on magnetic nanorods, Nanoscale 12 (18) (2020) 10090–10097.
[71] K.P. Sigdel, A.E. Pittman, T.R. Matin, G.M. King, High-resolution AFM-based force spectroscopy, Methods Mol. Biol. 1814 (2018) 49–62.
[72] G.M. King, J.A. Golovchenko, Probing nanotube-nanopore interactions, Phys. Rev. Lett. 95 (21) (2005), 216103.